Life Estimation of HVdc Cable Insulation Under Load Cycles: From Macroscopic to Microscopic Charge Conduction Modeling

Bassel Diban, *Member, IEEE*, and Giovanni Mazzanti, *Fellow, IEEE*

***Abstract*—This article goes one step forward in the life estimation of HVdc cable insulation under load cycles by introducing for the first time a microscopic model of charge conduction and transport, i.e., bipolar charge transport (BCT) model, for electric field calculation inside the insulation thickness. This article first includes the development and the validation of the BCT model with that found in the literature. Then, the parameters of the developed BCT model are optimized using pulsed electroacoustic (PEA) space charge measurements. Followed by the integration of the developed, validated and optimized model into the electric field calculation for life estimation of a 500-kV dc-XLPE insulated cable subjected to type test (TT) load cycles according to Cigrè Technical Brochure 852. The developed microscopic model is compared to the macroscopic models already found in the literature. The microscopic model shows a comparable electric field inversion similar to macroscopic models. However, the behavior of the microscopic model is noticed to be different under heating and cooling load cycles. In the hot cable, the maximum electric field stabilizes at different amplitudes and positions inside the insulation thickness in both models. This investigation has been carried out in the framework of the HEU-NEWGEN research project.**

***Index Terms*—Electric field, HVdc transmission, insulation, life estimation, modeling, power cable.**

I. Introduction

THE reliability of high-voltage direct-current (HVdc) cables has received increasing attention during recent decades as a result of the widespread adoption of HVdc cable systems, as well as the expansion of renewables deployment worldwide [1]. Life and reliability estimation has been developed to predict the life loss in cable insulation after being subjected to various stresses, i.e., electrical, thermal, mechanical, and environmental [2]. Electrothermal life models are mostly used in the literature both in cable design and in the estimation of remaining life [2], [3], [4], [5]. Those models and their relevant parameters [e.g., voltage endurance coefficient (VEC)] can be verified experimentally using accelerated life tests (ALTs) performed at high electric fields, whose results need to be carefully processed by ad hoc statistical tools under the Weibull hypothesis for breakdown strength and failure time distributions [6]. Although the empirical electrothermal life models are considered the most direct approach of life estimation, they are highly dependent on variables that are difficult to calculate straightforwardly, i.e., the temperature and the electric field distributions inside the insulation thickness. Two methods of electric field calculation were introduced in the literature, i.e., macroscopic and microscopic models of charge conduction. The macroscopic models are described by an analytical closed-form dependence of the electrical conductivity on temperature and electric field [7], while the microscopic models physically describe the charge conduction processes, i.e., injection, mobility [8], trapping, detrapping, and recombination as in the bipolar charge transport (BCT) model [9] whose parameters are usually derived using space charge measurements and/or conductivity measurement over time [10], [11].

So far, the authors have only used the macroscopic models of electrical conductivity for electric field calculation within a procedure developed for estimating life and reliability of HVdc cables subjected to load cycles [3], [4], [12], [13]. This article employs, for the first time, microscopic models of charge conduction and transport in such a procedure. Let us emphasize that this is the first necessary step toward the complete implementation of the BCT in the procedure. In particular, the main goal of this article is to apply the BCT model within the life estimation procedure for HVdc cables under load cycles using microscopic conduction phenomena—instead of the already used macroscopic approach—for electric field calculation in the insulation of a full-scale HVdc cable, thereby enabling a proper comparison with the already used macroscopic conduction models.

In this first step, some simplifying hypotheses are of course needed to relax the overall calculation complexity and address the main effects of charge injection and transport—described by the BCT for the bipolar charges considered here—on the electric field distribution within cable insulation thickness. This is why the microscopic conduction model treated here focuses on bipolar electronic charges and does not consider

Received 22 May 2025; revised 16 October 2025; accepted 12 December 2025. Date of publication 17 December 2025; date of current version 18 June 2026. This work was supported in part by European Union under Agreement 101075592. *(Corresponding author: Bassel Diban.)*

The authors are with the University of Bologna, 40136 Bologna, Italy (e-mail: bassel.diban2@unibo.it; giovanni.mazzanti@unibo.it).

Digital Object Identifier 10.1109/TDEI.2025.3645749

ionic species resulting, e.g., from cross-linking by-products, and aging, as more deeply commented in Section VII.

The research methodology here is based on developing the BCT model and optimizing its parameters under controlled laboratory conditions on clean state-of-the-art XLPE flat specimens in order to isolate and investigate purely electronic conduction phenomena. The deployed methodology ensures the derivation of the nonlinear model parameters with the least interference from cross-linking by-products. For this reason, BCT model parameters are derived from space charge measurements on thin flat samples; as pointed out above, for the sake of simplicity in this first step, the effects of scaling up electrical characterization from flat specimens to full-size cable insulation, e.g., impurities and role of semiconductors, are not treated.

This article is organized as follows.

1) Section II, the microscopic BCT model is developed as in the literature [9], [14].
2) Section III, the microscopic BCT model and the resulting electric field are validated using a replicated case study as in [9] and [14].
3) Section IV, the BCT model parameters are found using an ad hoc MATLAB[1] optimization process with the space charge measurements carried out on cross-linked polyethylene dedicated for dc cables (dc-XLPE).
4) Section V, the developed and optimized BCT model is included in the electrothermal life and reliability estimation procedure to calculate the electric field.
5) Section VI reports the results of a long space charge measurement under a load cycle for experimental validation of the simulation.
6) Section VII includes an in-depth discussion of the main similarities and differences between both microscopic and macroscopic models, as well as the resulting electric field distributions.
7) Section VIII is a conclusion that highlights the main findings and future research.
8) Appendix includes details about the space charge measurements carried out on dc-XLPE together with the pattern of the optimized BCT model at each temperature, electric field, and voltage polarity.

This investigation has been performed in the framework of the WP4 “Tools and models for reliable and resilient HVdc cable systems” of the HEU-NEWGEN research project.

II. BCT Model Development

The BCT model includes the following physical processes [9], [11], [14]:

1) the injection of charge carriers from the electrodes into the insulation, represented here by Schottky injection of both electrons and holes, as in (1);
2) the mobility of charge carriers from the vicinity of the injecting electrode toward the opposite electrode [see (2) and (3)];
3) various physical processes that lead to a variation in the charge density, i.e., trapping, detrapping, and recombination of charge carriers [see (4)–(12)]

$$J_{\mathrm{sch}\,e,h} = A_0 T^2 \exp\left(-\frac{w_{e,hi}}{k_B T}\right) \times \left[\exp\left(-\frac{e}{k_B T}\sqrt{\frac{eE}{4\pi\varepsilon}}\right) - f_s\right] \tag{1}$$

$$\mu_{e,h} = \frac{2\upsilon a}{E}\exp\left(-\frac{w_{\mu_{e,h}}}{k_B T}\right)\cdot \sinh\left(\frac{qaE}{2k_B T}\right) \tag{2}$$

$$\upsilon = \frac{k_B T}{h}. \tag{3}$$

Source terms are given by the following equations:

$$s_{e,\mu} = -B_e\rho_{e,\mu}\left(1-\frac{\rho_{e,t}}{\rho_{e0t}}\right) + D_e\rho_{e,t} - S_1\rho_{e,\mu}\rho_{h,t} - S_3\rho_{e,\mu}\rho_{h,\mu} \tag{4}$$

$$s_{e,t} = B_e\rho_{e,\mu}\left(1-\frac{\rho_{e,t}}{\rho_{e0t}}\right) - D_e\rho_{e,t} - S_0\rho_{e,t}\rho_{h,t} - S_2\rho_{e,t}\rho_{h,\mu} \tag{5}$$

$$s_{h,\mu} = -B_h\rho_{h,\mu}\left(1-\frac{\rho_{h,t}}{\rho_{h0t}}\right) + D_h\rho_{h,t} - S_2\rho_{h,\mu}\rho_{e,t} - S_3\rho_{e,\mu}\rho_{h,\mu} \tag{6}$$

$$s_{h,t} = B_h\rho_{h,\mu}\left(1-\frac{\rho_{h,t}}{\rho_{h0t}}\right) - D_h\rho_{h,t} - S_0\rho_{h,t}\rho_{e,t} - S_1\rho_{h,t}\rho_{e,\mu} \tag{7}$$

where

$$S_0 = S_{0,\mathrm{base}} \tag{8}$$

$$S_1 = S_{1,\mathrm{base}} + \frac{\mu_e}{\varepsilon} \tag{9}$$

$$S_2 = S_{2,\mathrm{base}} + \frac{\mu_h}{\varepsilon} \tag{10}$$

$$S_3 = S_{3,\mathrm{base}} + \frac{\mu_e + \mu_h}{\varepsilon} \tag{11}$$

$$D_{e,h} = \upsilon \exp\left(-\frac{w_{tr\,e,h}}{k_B T}\right). \tag{12}$$

Current continuity equations are derived in the following:

$$\nabla\cdot(J_{\mathrm{drift}} + J_{\mathrm{diff}}) + \frac{\partial\rho_{e,h}}{\partial t} = s_{e,h\,\mu,t}. \tag{13}$$

Drift current density is written as follows:

$$J_{\mathrm{drift}\,e,h\mu}(r,t) = \mu_{e,h}(r,t)\,\rho_{e,h\mu}(r,t)\,E(r,t). \tag{14}$$

Diffusion current density is given by

$$J_{\mathrm{diff}\,e,h\mu}(r,t) = D_{\mathrm{diff}}\nabla\left(\rho_{e,h\mu}\right) \tag{15}$$

$$D_{\mathrm{diff}} = \frac{k_B T}{q}\mu_{e,h}. \tag{16}$$

The net charge density is given as follows:

$$\rho_{\mathrm{net}} = -\rho_{e,\mu} + \rho_{h,\mu} - \rho_{e,t} + \rho_{h,t}. \tag{17}$$

The electric field is calculated from

$$\nabla\cdot(\varepsilon_0\varepsilon_r \boldsymbol{E}) = \rho_{\mathrm{net}} \tag{18}$$

[1]Trademark.

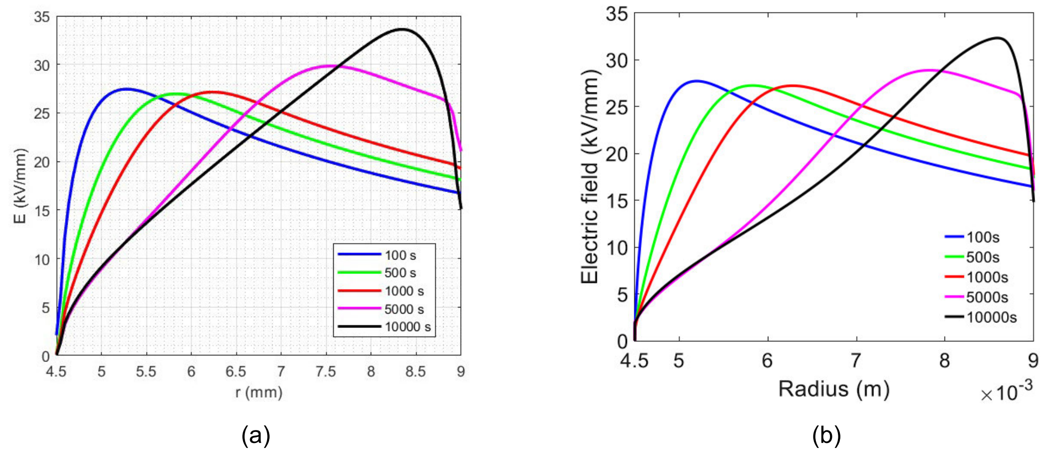

Fig. 1. Electric field distribution for the validation of the BCT model developed in this work (a) with that developed in Roy et al. [9] and Zhan et al. [14] and (b) having the same temperatures, cable geometry, and applied voltage.

where S_0, S_1, S_2, and S_3 are the recombination coefficients and $S_{0,\text{base}}$ is the base level for trapped hole-trapped electron recombination, which exhibits no velocity/field dependence, as both carriers are stationary. $S_{1,\text{base}}$, $S_{2,\text{base}}$, and $S_{3,\text{base}}$ are base level recombination rates for trapped hole–mobile electron, mobile hole–trapped electron, and mobile electron–mobile hole recombination, respectively. υ attempts to escape frequency; h is Planck's constant. B_e and B_h are trapping coefficients for electrons and holes, respectively. $\mu_{e,h}$ is the mobility of charges. w_{μ_a} is the depth of a single trapping level for mobility (eV). a is the average distance between traps. $D_{e,h}$ are the detrapping coefficients for electrons and holes, respectively. ρ_{e0t} and ρ_{h0t} are the maximum trapped charge densities for electrons and holes, respectively. J is the conduction current density (A/m^2). The subscripts μ and t refer to mobile and trapped charges, respectively. ρ refers to the charge density (C/m^3), ρ_{net} is the net charge density at a generic point and time instant (C/m^3), and E is the electric field (kV/mm).

III. BCT Model Validation

The BCT model—developed in this study and used for electric field calculations and life estimation under dc conditions—has been validated using the results of similar simulations found in the literature by Roy et al. [9] and Zhan et al. [14]. A 4.5-mm-thick 90-kV XLPE cable insulation is used for model validation. This validation used the finite difference method (FDM) with 100 mesh points inside the cable insulation for BCT and electric field calculations. Temperature drop inside the insulation is generated by the thermal ohm's law between $T(r_i) = 65$ °C and $T(r_o) = 45$ °C, respectively,

$$T(r) = T(r_i) - [T(r_i) - T(r_o)] \ln\left(\frac{r}{r_i}\right) \Big/ \ln\left(\frac{r_o}{r_i}\right). \quad (19)$$

Five time points are considered for plotting the electric field, i.e., 100, 500, 1000, 5000, and 10 000 s, for the sake of comparison. Fig. 1 shows the comparison between the electric fields calculated from the BCT model developed in this study [in Fig. 1(a)] with those calculated from the model developed in [9] and [14] [in Fig. 1(b)]. The electric field distributions are in quite good agreement with a maximum electric field of 33.5 kV in this model compared to 32.7 kV reported in the literature. The relative error, which does not exceed 2.5%, can be deemed conservative.

IV. BCT Model Parameters Optimization

The parameters of the microscopic model are investigated by iterative fitting of MATLAB simulations in comparison with the charge density measured using the pulsed electroacoustic (PEA) space charge measurement carried out on dc-XLPE. The 200-μm-thick hot-pressed dc-XLPE specimens were produced by the VTT Research Center of Finland, coordinator and partner of the HEU-NEWGEN research project. Then, the specimens were degassed in a vacuum oven at 70 °C for 48 h to remove the cross-linking by-products. The PEA space charge measurements were carried out at the University of Bologna, Italy (leader of WP4 of the HEU-NEWGEN research project) under different temperatures, electric fields, and polarity of the applied voltage. However, the space charge measurement during the volts-on period shows—in addition to the trapped/mobile space charges inside the specimen—induced charges on the electrode that cannot be represented by the BCT model. Therefore, capacitive and image surface charges are superimposed on the simulation results to be comparable with the experimental data [10], [15]

$$n_{\text{cap}} = \pm \varepsilon E_{\text{mean}} \quad (20)$$

$$n_{im}(-) = -\frac{1}{x_d} \sum_{i=1}^{i=d-1} \rho_{x_i} \cdot (x_d - x_i) \cdot \Delta x_i \quad (21)$$

$$n_{im}(+) = -\frac{1}{x_d} \sum_{i=1}^{i=d-1} \rho_{x_i} \cdot (x_i) \cdot \Delta x_i \quad (22)$$

where n_{cap} is the capacitive contribution to surface charges (C/m^2), n_{im} is the image surface charges (C/m^2), and x_i is the distance at the point i from the cathode. x_d is the insulation thickness divided into $d - 1$ intervals. Δx_i is the interval distance. ρ_{x_i} is the volume charge density (C/m^3).

Fig. 2 shows a flowchart that illustrates the optimization algorithm. The optimization depends on the nonlinear

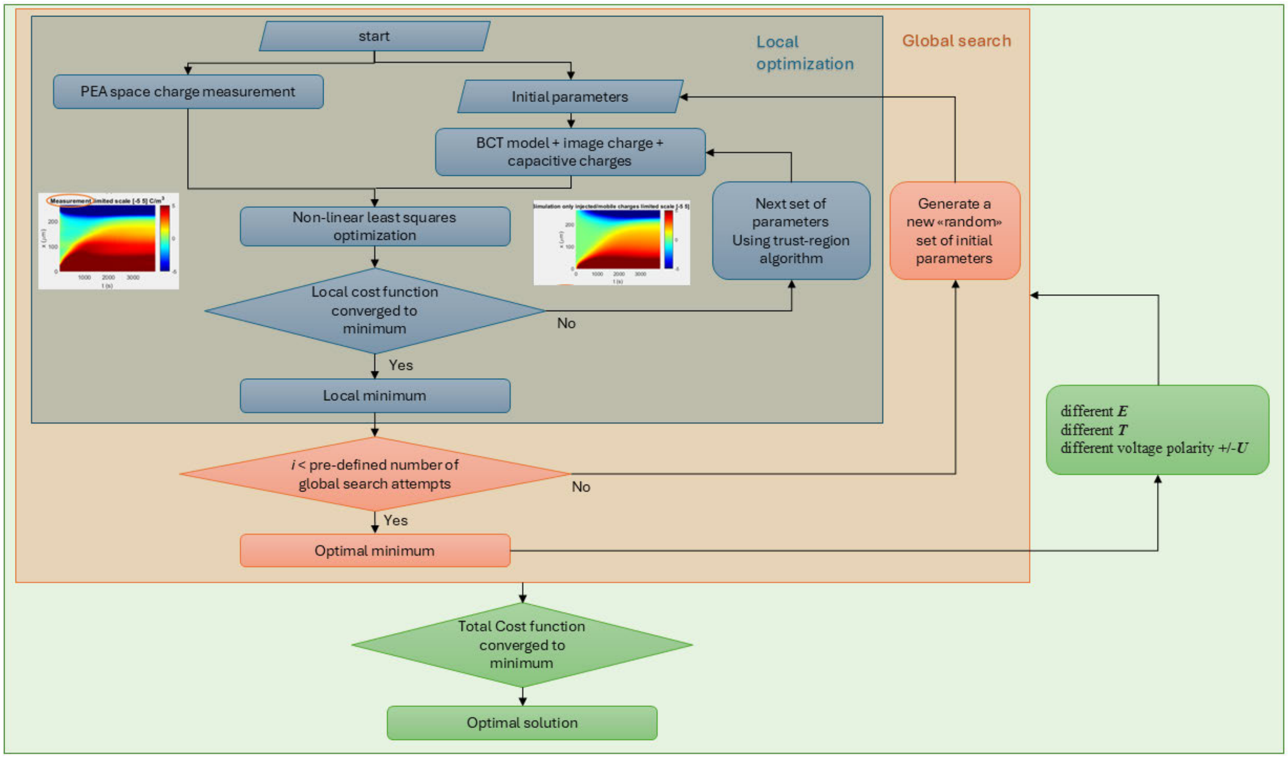

Fig. 2. Algorithm for local and optimal (best-known) minimum search for the parameters of the BCT model.

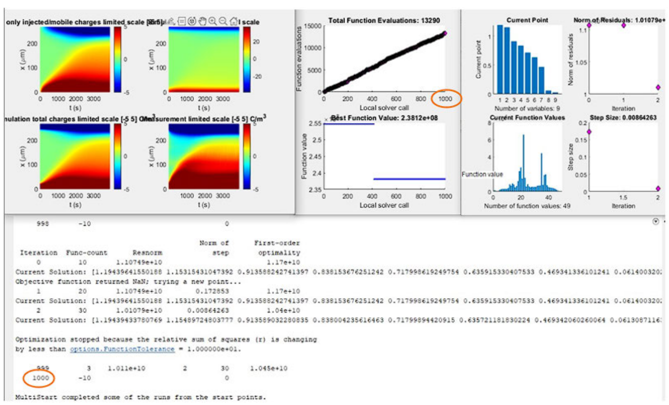

Fig. 3. Optimization GUI window evolution during the optimization process at E = +40 kV/mm and T = 20 °C for dc-XLPE from the HEU-NEWGEN project.

least squares optimization, which searches for the parameters that lead to the minimum of the sum of the squared differences between the space charge measurement and the simulation. The minimization of the cost function is achieved using the trust-region algorithm [10]. MATLAB is used for both the simulation and the optimization processes. An ad hoc graphic user interface (GUI) has been developed to follow the evolution of the optimization process at each iteration (as in Fig. 3).

The insulation thickness in the simulation is divided into 50 points; similarly, the measured data are interpolated to give 50 points inside the insulation thickness. The duration of the measurement considered for the optimization is ≈ 4000 s as a compromise between the stability of the pattern of the space charge measurement and the duration of each iteration during the optimization process of the simulation parameters. In the optimization code, the BCT model discretization is modified to consider for flat geometry to be compared with the space charge pattern in flat specimens. The local minimum is the first minimum at which the algorithm arrives, starting from the initial parameters. The optimal minimum is the best-known minimum as a result of the repetition of the same algorithm starting from a predefined range of a random set of initial parameters in one E and T set. A total cost function is used to find the optimal solution over all E and T combinations [10].

Fig. 3 shows the GUI evolution during the optimization process at E = +40 kV/mm and T = 20 °C for dc-XLPE specimens from the HEU-NEWGEN project. For more details about the optimization results, Figs. 9–12 show the patterns of the PEA measurement [in Figs. 9(a)–12(a)] in comparison with the optimized parameters [in Figs. 9(b)–12(b)] at different temperatures, electric fields, and polarities of the applied voltage.

Table I shows the optimization result of the parameters of the BCT model for dc-XLPE specimens from the HEU-NEWGEN project as a function of electric field E (ranging from −30 kV/mm) and temperature T (ranging from 20 °C to 50 °C). Higher temperatures (including the design temperature of the state-of-the-art HVdc cables) result in a very fast charge dynamic pattern that cannot be recognized by the optimization algorithm. It can be noticed from Table I that the optimized parameters show comparable injection and mobility (energy barriers) for both electrons and holes compared to the parameters found in the literature, in the sense that the optimized parameters exhibit fairly similar values for electrons and holes, while the literature param-

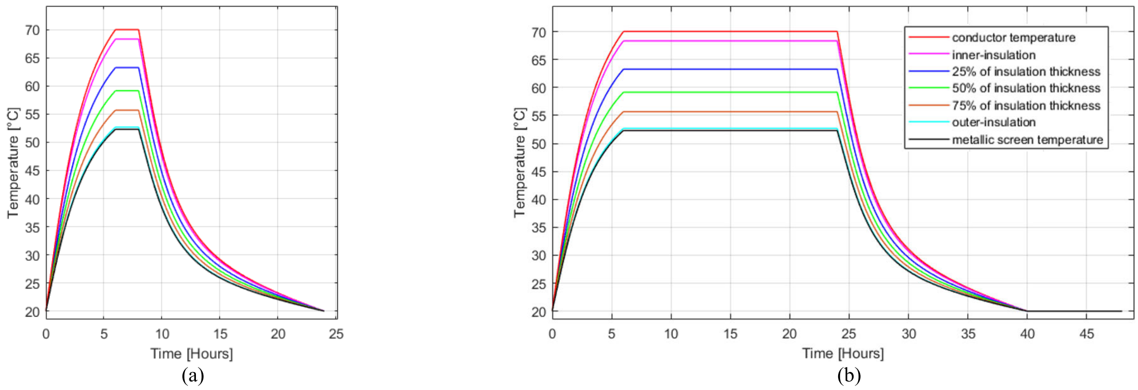

Fig. 4. Temperature profile during (a) 24- and (b) 48-h TT load cycles for five radial points inside the insulation thickness of the case-study cable according to [16].

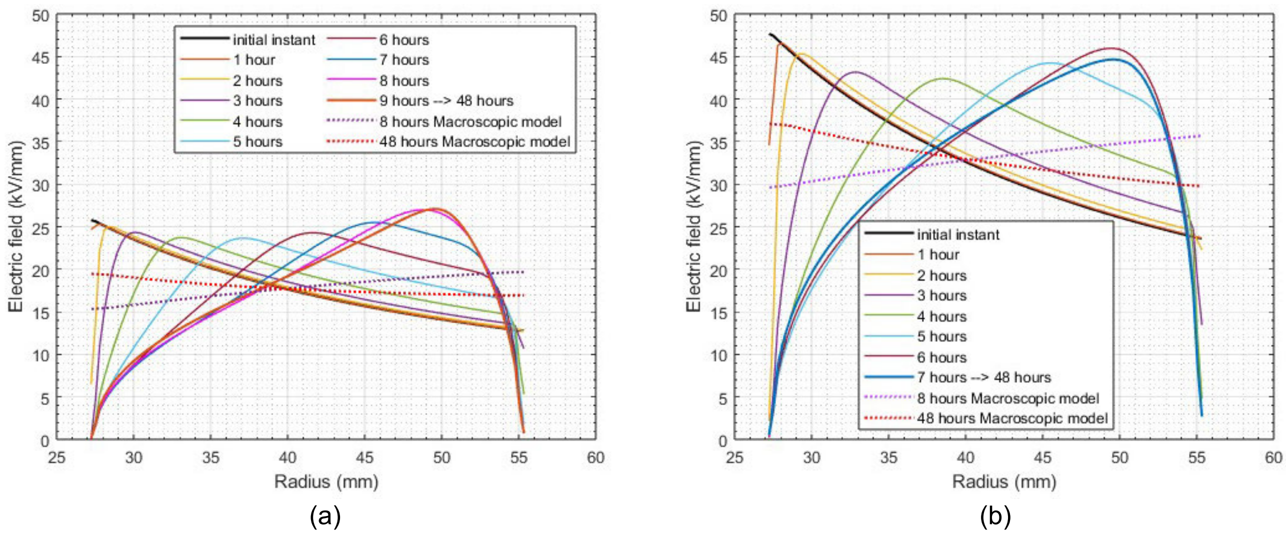

Fig. 5. Transient electric field distribution inside the insulation thickness of the case-study cable during a 48-h load cycle under (a) rated voltage U_0 and (b) TT voltage U_{TT}.

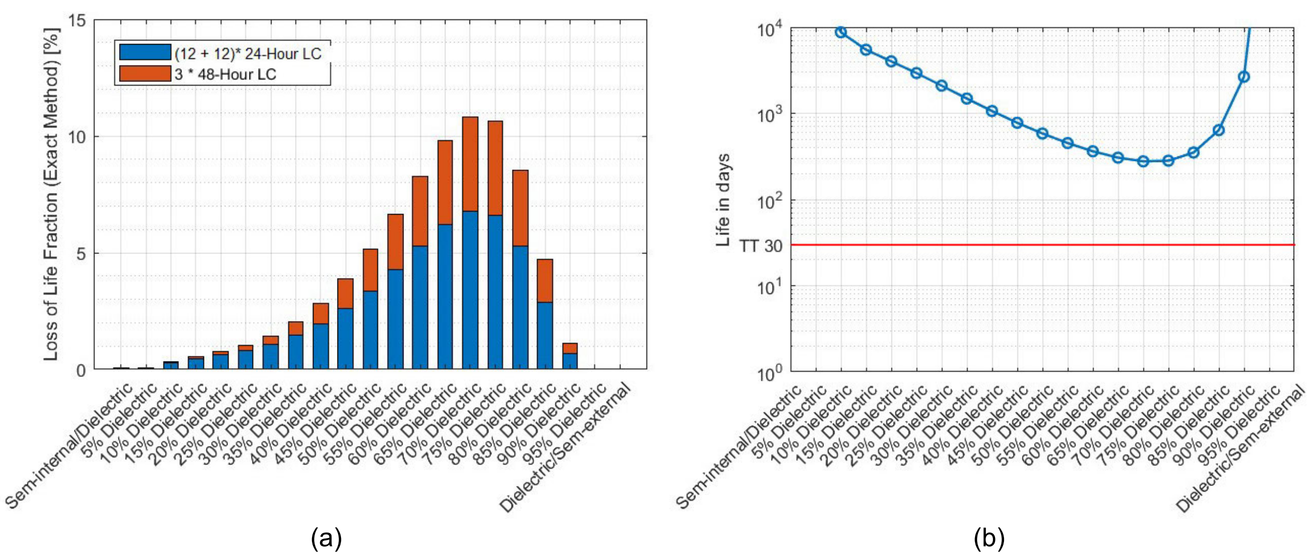

Fig. 6. (a) Percent loss of life fractions inside the insulation thickness of the case-study cable under the TT conditions during all 24-h load cycles (blue bars) and 48-h load cycles (red bars). (b) Life distribution (in days) inside the insulation thickness of the case-study cable under the TT conditions.

eters are more different for electrons and holes. The latter might be justified by the inclusion of the negative polarity of the applied voltage in the optimization, which reduces the geometrical and material effect of the PEA test cell elec-

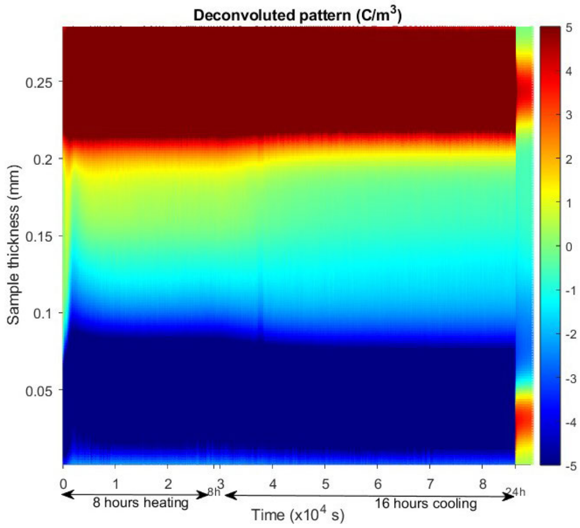

Fig. 7. Space charge measurement on dc-XLPE flat specimen subjected to 24-h load cycle (8-h heating followed by 16-h cooling).

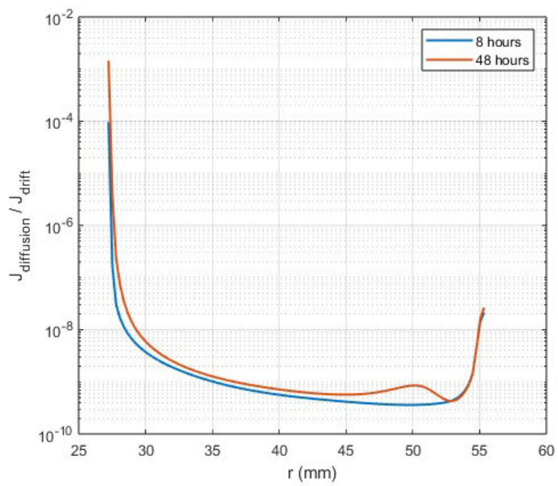

Fig. 8. Ratio between diffusion current density/drift current density inside the insulation for hot and cold cables during the load cycle.

TABLE I
OPTIMIZED PARAMETERS OF THE BCT MODEL FOR DC-XLPE FROM THE HEU-NEWGEN PROJECT

	E (kV/mm)	T (°C)	w_{ei} (eV)	w_{hi} (eV)	w_{tre} (eV)	w_{trh} (eV)	w_{ue} (eV)	w_{uh} (eV)	B_e (1/s)	B_h (1/s)	S_{base} (m^3/s.C)
Initial	--	--	1.18	1.19	0.84	0.91	0.671	0.652	0.29	0.16	0.047
Local min and global search	-30	20	1.18	1.18	0.84	0.91	0.672	0.652	0.30	0.16	0.046
	+30		1.20	1.18	0.91	0.85	0.659	0.653	0.17	0.30	0.046
	+40		1.20	1.14	0.92	0.84	0.654	0.686	0.15	0.29	0.042
		50	1.22	1.22	0.90	0.89	0.687	0.682	0.40	0.49	0.048
Optimal solution	Multi E, T and polarities		1.22	1.20	0.91	0.90	0.684	0.680	0.30	0.30	0.045
Literature values [9]			1.27	1.16	0.96	0.99	0.71	0.65	0.1	0.2	-
Literature values [10]			1.21	1.1	-	-	0.71	0.6	0.2	0.9	-
Literature values [11]			0.905	1.148	1.03	1.03	0.76	0.74	-	-	0.0001

trodes. The optimized parameters will be further considered in the electric field calculation for the life estimation in Sections V–VII.

TABLE II
CASE-STUDY CABLE CHARACTERISTICS

Parameter	**value**
Rated power (monopolar scheme) (MW)	960
Rated current, I_n (A)	1920
Conductor Material	Cu
Conductor cross-section (mm^2)	2000
Rated voltage, U_0 (kV)	500
Conductor design temperature T_D (°C)	70
Insulation Material	DC-XLPE
relative permittivity ε_r	2.3
Inner semiconductor thickness (mm)	2
Insulation thickness (mm)	28.1
Outer semiconductor thickness (mm)	1
Metallic shield thickness (mm)	1
Thermoplastic sheath thickness (mm)	4.5
Burial depth bb (m)	1.3
Design value of soil resistivity (m.K/W)	1.3
Ambient temperature (°C)	20
Design life L_D (years)	40
Design failure probability P_D (reliability R_D) %	1 (0.99)
n_D IPM exponent at design temperature	10
B Arrhenius model parameter (K)	12430
b_{ET} electro-thermal synergism parameter (K)	0

V. CASE STUDY FOR LIFE ESTIMATION

A. Cable Characteristics

The case study investigates the electrothermal life of a 500-kV-HVdc extruded cable subject to the type test (TT) load cycles according to [16]. The main electrical and thermal characteristics of the case-study cable, as well as the parameters of the electrothermal life model used for their dc-XLPE insulation, can be found in Table II.

B. Temperature Profile

The cable is subjected to the TT load cycles according to CIGRÉ Technical Brochure 852 [16]. The TT load cycles consist of 24 consecutive cycles of the 24-h type, followed by three cycles of the 48-h type. Fig. 4 shows the temperature profile at five points inside the insulation thickness during the 24-h load cycle [in Fig. 4(a)] and 48-h load cycle [in Fig. 4(b)].

C. Electric Field Calculation

The transient electric field profiles $E(r, t)$ are calculated during one load cycle of the LC period at 100 mesh points (i.e., the discrete spatial radial positions of the FDM mesh inside the insulation) inside the insulation of the studied cable during both 24- and 48-h load cycles LCs. Two methods are used for the calculation:

1) the microscopic method consisting of solving BCT (1)–(18) for the BCT parameters obtained during the NEWGEN project and reported in Table I (solid lines in Fig. 5);
2) the macroscopic method based on the solution of Maxwell's equations with Klein's closed-form dependence of the electrical conductivity on temperature and

electric field, shown in (23) (represented by the dotted lines in Fig. 5)

$$\sigma = \frac{J_{\text{drift}}}{E} = \sigma_0 \exp(aT + bE) \quad (23)$$

where σ_0 is the theoretical value of σ at 0 °C and for an electric field equal to 0 kV/mm and a and b are the temperature and field coefficients of electrical conductivity, respectively [13].

With the microscopic method, Fig. 5 shows that the electric field profile within cable insulation starts from the Laplacian field at the beginning of the cycle, and then, it takes approximately 9 and 7 h at both the rated voltage U_0 and the TT voltage U_{TT}, respectively, to arrive at a steady-state field distribution, which is then kept until the end of the 48-h load cycle. This result is different compared to that obtained with the macroscopic method, where the electric field profile within cable insulation during the 48-h load cycle changes from the Laplacian at the beginning to the "hot cable" field distribution in the highest temperature part of the cycle (see the dashed line at 8 h, where the field profile is completely inverted) and then back to the "cold cable" field distribution in the lowest temperature part of the cycle (see the dashed line at 48 h, where the field profile is not inverted).

The most electrically stressed point inside the insulation starts at the inner insulation at the beginning of the *LC* because of the Laplacian electric field in the cylindrical cable geometry; then, over time, the most stressed point shifts toward the outer insulation until it arrives to ≈ 70% of the entire insulation thickness at 9 and 7 h at both the rated voltage U_0 and the TT voltage U_{TT}, respectively. Thereafter, the most stressed point remains there throughout the cycle. Also, this result is different from that obtained with the macroscopic method, where the most stressed point—consistently with the whole electric field profile—during 48-h load cycles changes from the outer insulation surface for the "hot cable" in the highest temperature part of the cycle (dashed line at 8 h) to the inner insulation surface for the "cold cable" in the lowest temperature part of the cycle (dashed line at 48 h).

The longer time to steady-state field obtained at U_0 (9 h) compared to U_{TT} (7 h) is easily explained via the macroscopic conductivity approach since the value of dielectric time constant $\tau = \varepsilon/\sigma(E,T)$ is expected to be greater for the lower voltage U_0 compared to U_{TT}: indeed, at a given temperature, the greater the voltage and the field E, the greater the conductivity $\sigma(E,T)$ and the smaller the dielectric time constant τ.

D. Life Estimation

The electrothermal IPM-Arrhenius life model of (24) is used to assess the lifespan of the dc-XLPE cable insulation under TT conditions. Specifically, cast into the Miner's law framework of aging accumulation over time [13] as per the following (25)–(27), it estimates the accumulated loss of life $LF_{\text{cycle}}(r)$ and the time-to-failure $L_{\text{cycle}}(r)$ versus insulation radius r during TT load cycles, as well as the life of the most stressed point in the insulation L_{cycle}

$$L(E,T) = L_D \cdot [E/E_D]^{-(n_D - b_{ET}T'')} [E_D/E_0]^{b_{ET}T''} e^{-BT''} \quad (24)$$

$$LF_{\text{cycle}}(r) = \int_0^{t_d} \frac{dt}{L[E(r,t), T(r,t)]} = \frac{1}{K_{\text{cycle}}(r)} \quad (25)$$

$$L_{\text{cycle}}(r) = t_d \times K_{\text{cycle}}(r) \quad (26)$$

$$L_{\text{cycle}} = \min\{L_{\text{cycle}}(r), r \in [r_i, r_o]\} \quad (27)$$

where L is life at dc electric field E and temperature T, $T'' = 1/T_D - 1/T$ (E_D, T_D, and L_D being design electric field, temperature, and life, respectively), n_D is the value of VEC at T_D, b_{ET} is the synergism factor between the electrical and thermal stress, $B = \Delta W/K_B, \Delta W$ is the activation energy of the main thermal degradation reaction, $K_B = 1.38 \times 10^{-23}$ J/K is Boltzmann's constant, and $K_{\text{cycle}}(r)$ is the number of cycles-to-failure at a generic radius r. Further details about the detailed temperature calculations, macroscopic electric field calculation, and life estimation are omitted here for the sake of brevity and can be found in [2], [4], and [12].

Fig. 6(a) shows the loss of life distribution inside the insulation thickness of the case-study cable during 24-h LCs in blue bars and 48-h LCs in red bars, obtained using the BCT model, while Fig. 6(b) shows the life of cable (in days) inside the insulation thickness of the case-study cable under the TT conditions. Consistent with the field profiles reported in Fig. 5(a) and (b), the most stressed point, i.e., the one with the highest loss of life, corresponds to 70% of the insulation thickness at a maximum loss of life = 13%. A quite significant loss of life is associated with the 3 × 48-h load cycles, compared to the 24 × 24-h load cycles.

In Fig. 6(b), the minimum life point, corresponding to 70% of the insulation thickness, represents the life of the cable according to the BCT model and is still greater than the duration of the TT. Therefore, the cable is expected to withstand TT according to the life estimation using the BCT model. The same was concluded in [13] for a 500-kV cable using the macroscopic conductivity approach, except for the position of the maximum stress point inside the insulation, where it is always placed either at the inner insulation or at the outer insulation in the case of macroscopic models, as hinted at above.

VI. Experimental Validation

A long space charge measurement on a 0.22-mm-thick dc-XLPE flat specimen subjected to 35 kV/mm and one 24-h load cycle (8-h heating followed by 16-h cooling) is carried out (see Fig. 7) to validate the *LC* simulation results on the same XLPE insulation. Charge dynamics can be noticed during the first 2 h, and then, the charge pattern is stabilized even during the 16-h cooling period. The results show that space charge variation during the cooling period is minor and mainly affects the electrodes' vicinity. The results agree with other space charge measurement patterns carried out on thick ac-XLPE cables [17], [18], where the space charge and electric field variations are minor during the cooling period of the load cycle, while the results in this article are not fully comparable to the raw PEA signal of a full-size HVdc cable under load cycles [19]. To link the experimental result with the simulated results, both the electronic diffusion current density and the drift current density are calculated as in (14) and (15). Fig. 8 shows the electronic diffusion current density/drift current density ratio

TABLE III
CHARACTERISTICS OF MACROSCOPIC AND MICROSCOPIC CHARGE CONDUCTION MODELS

	Macroscopic	Microscopic
Source term	$\nabla \cdot J + \frac{\partial \rho}{\partial t} = 0$	$\nabla \cdot J_{e,h} + \frac{\partial \rho_{e,h}}{\partial t} = s_{e,h}$
Conductivity dependency	$f(E,T)$	$f(\mu_{e,h}, \rho_{e,h\,\mu})$
Space charge distribution	linear	Non-linear
Memory of generated space charges	Memory-less	Has a memory
Electric field inversion	Present and moderate	Present and strong
Electric field response to heating-cooling load cycles	Significant	Minor or no change
Maximum electric field position	Either at inner or outer insulation	Can be inside the insulation

inside the insulation thickness for hot and cold cables (at 8 and 48 h during the load cycle, respectively). It shows that diffusion current density is lower than drift current density by three to nine orders of magnitude. Thus, the drift conduction dominates the electric field distribution although the diffusion is present in the high charge density gradient zones.

VII. Discussion

Space charge accumulation is considered a key parameter in determining the performance of a certain insulating material in dc systems. The main reason is the dependence of the electric field distribution on the space charges accumulated inside the insulation, as the poling dc field causes space charge injection, mobility, trapping, and/or detrapping inside the cable insulation, hence changing the capacitive electric field distribution into a more complicated field distribution, dissimilar to the ac system where the electric field is still capacitive due to the absence of such space charge accumulation and mobility. Physical models for describing the space charge behavior inside the insulation are developed with the proper fitting parameters to the space charge measurements (e.g., BCT model). Another simpler method for describing the space charge behavior is to be represented by the macroscopic electrical conductivity in a phenomenological way, where the electrical conductivity is expressed by means of a closed-form function of the temperature and electric field. Then, the charge density can be calculated as the charges accumulated at the discontinuities of permittivity and conductivity. The former methods are called physical (or microscopic) models, while the latter are called phenomenological (or macroscopic) models for charge conduction. Macroscopic and microscopic models of charge conduction are characterized in this article, as reported in Table III. It shows the effect of the source term in the continuity equation that serves as a memory of the physical processes inside the insulation represented by charge trapping, charge detrapping, and charge recombination, described by (4)–(7), in the BCT model, while, in the macroscopic conduction, the absence of the source term in the continuity equation eliminates the memory effect of the model. In addition, the drift current density in the BCT model is related to the space charge density, as in (14), while it has a phenomenological relation to the electric field and temperature in the macroscopic models, as in (23).

Fig. 5 shows that, according to the BCT, the cooling period has no effect on the electric field distribution, dissimilar to the electric field derived from macroscopic models, which varies according to temperature variation during the load cycle. This response can be justified by the memory dynamic effect of the microscopic models that depend on the history of space charges variation compared to the memory-less macroscopic models that depend only on the electric field and temperature, as already illustrated in Table III.

Results show that even considering electronic charge diffusion with various diffusion parameters shows no variation of the electric field during the cooling period of the load cycle as long as the voltage is still applied. Electronic charge diffusion has been deemed negligible in [10] and [20], while it shows noticeable charge relaxation in [11], however, in a thin specimen over many hours and when the voltage is off.

The space charge pattern during the load cycle plays a critical role in the reliability and life estimation of HVdc cables, as its cumulative effect over multiple load cycles can significantly influence the electric field distribution, thereby impacting the overall life of the cable. For this reason, future simulative and experimental investigations are needed to verify potential charge relaxation phenomena that might affect space charge storage and, thereby, the electric field distribution during the load cycle. This includes considering other BCT model developments, e.g., a distributed energy level of traps, as in [21].

As a closing remark, let us further highlight that in this case, the utilization of degassed flat specimens for the optimization of the BCT model parameters is well justified, as the adopted methodology ensures accurate extraction of the nonlinear model parameters while minimizing interference from cross-linking by-products; since the optimization procedure is highly sensitive to charge injection and mobility patterns, the presence of additional ionic charges cannot be distinguished by the algorithm. In the case of full-scale XLPE cable insulation where a higher concentration of crosslinking by-products is present in the insulation, additional physical and chemical phenomena, such as ion formation and mobility [22], must be integrated into the modeling framework. Addressing these effects requires other measurement techniques and modified optimization models to minimize the interference with electronic injection and transport processes. Upscaling the results to provide a comprehensive representation of the full-size cable is beyond the scope of this first-step preliminary study and will be considered in subsequent steps as the main goal of future research activities. This will require accounting also for the ionic species that represent the cross-linking byproducts in the BCT model [23]. Since the model investigated in this article considers the sole electronic drift and diffusion mobility, electronic and ionic charge diffusion are also to be investigated experimentally in future research.

VIII. Conclusion

This article studies the electrothermal life estimation in HVdc cables, considering the microscopic models of charge conduction for the electric field calculation inside the insulation thickness. This article first develops and validates the BCT model using case studies found in the literature. Then, the BCT model is applied for the electric field calculation to be used in the electrothermal life estimation. The novelties in this article can be summarized as follows.

1) The parameters of the BCT model are found using an ad hoc optimization process in comparison with the experimental data coming from space charge measurements using the pulsed-electroacoustic method (PEA) on dc-XLPE flat specimens produced in the framework of the HEU-NEWGEN research project.
2) The parameters of BCT optimized in this article indicate comparable values of both injection and mobility of both holes and electrons, dissimilar to the parameters already found in the literature.
3) An in-depth analysis of the electric field distribution using microscopic and macroscopic models under heating and cooling load cycles is introduced for the first time. The main difference is that the electric field inversion is continuous during the consecutive load cycles when using the macroscopic model, while the electric field shows no variation after the first heating of the first load cycle when using the microscopic model. The memory effect of the space charges in the microscopic models can justify this pattern, which is extensively discussed in this article. In a hot cable, the maximum electric field point is shifted from the inner insulation to 70% of the insulation thickness using the microscopic model, while it is shifted to the outer insulation surface using the macroscopic model.
4) The electrothermal life estimation of a case-study HVdc cable under load cycles by means of the electric field calculated via the BCT has been performed for the first time here in the literature (using the optimized BCT parameters); similar to the results obtained with previously developed macroscopic models, greater life compared to the TT duration is obtained. This agrees with the fact that the well-designed HVdc cables should withstand the TT. The main difference between the macroscopic and microscopic models for the life estimation is the position and the amplitude of the most stressed point inside the insulation thickness. The nonlinearity of the space charge distribution in the case of microscopic models plays an important role in this difference, in comparison with the linear charge distribution in the case of macroscopic models.

Future research will focus on the development of the BCT model and the life estimation approach and parameters to consider novel HVdc cable insulations.

APPENDIX

See Figs. 9–12.

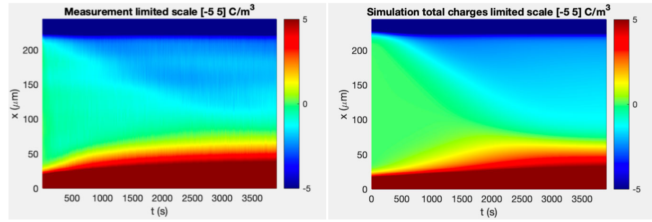

(a) (b)

Fig. 9. Space charge density (C/m^3) in a flat dc-XLPE specimen under negative polarity of the applied voltage (E = −30 kV/mm) and (T = 20 °C) according to (a) measurement and (b) optimized simulation from BCT.

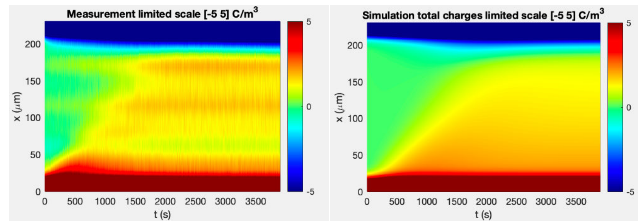

(a) (b)

Fig. 10. Space charge density (C/m^3) in a flat dc-XLPE specimen under positive polarity of the applied voltage (E = +30 kV/mm) and (T = 20 °C) according to (a) measurement and (b) optimized simulation from BCT.

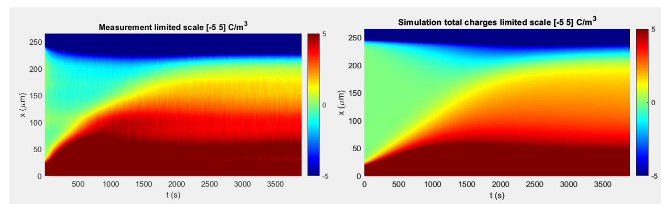

(a) (b)

Fig. 11. Space charge density (C/m^3) in a flat dc-XLPE specimen under positive polarity of the applied voltage (E = +40 kV/mm) and (T = 20 °C) according to (a) measurement and (b) optimized simulation from BCT.

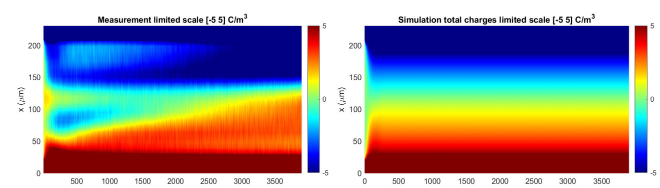

(a) (b)

Fig. 12. Space charge density (C/m^3) in a flat dc-XLPE specimen under positive polarity of the applied voltage (E = +40 kV/mm) and (T = 50 °C) according to (a) measurement and (b) optimized simulation from BCT.

ACKNOWLEDGMENT

Funded by the European Union Grant Agreement No 101075592. Views and opinions expressed are however those of the author(s) only and do not necessarily reflect those of the European Union or CINEA. Neither the European Union nor the granting authority can be held responsible for them.

Funded by the European Union

References

[1] G. Mazzanti, "Updated review of the life and reliability models for HVDC cables," *IEEE Trans. Dielectr. Electr. Insul.*, vol. 30, no. 4, pp. 1371–1390, Aug. 2023, doi: 10.1109/TDEI.2023.3277415.

[2] G. Mazzanti, "Life and reliability models for high voltage DC extruded cables," *IEEE Elect. Insul. Mag.*, vol. 33, no. 4, pp. 42–52, Jul. 2017, doi: 10.1109/MEI.2017.7956632.

[3] G. Mazzanti, "Life estimation of HVDC cables under the time-varying electrothermal stress associated with load cycles," *IEEE Trans. Power Del.*, vol. 30, no. 2, pp. 931–939, Apr. 2015.

[4] G. Mazzanti, "Including the calculation of transient electric field in the life estimation of HVDC cables subjected to load cycles," *IEEE Elect. Insul. Mag.*, vol. 34, no. 3, pp. 27–37, May 2018.

[5] B. Diban, G. Mazzanti, and P. Seri, "Life-based geometric design of HVDC cables—Part I: Parametric analysis," *IEEE Trans. Dielectr. Electr. Insul.*, vol. 29, no. 3, pp. 973–980, Jun. 2022, doi: 10.1109/TDEI.2022.3168369.

[6] G. Mazzanti, G. C. Montanari, and L. Simoni, "Insulation characterization in multistress conditions by accelerated life tests: An application to XLPE and EPR for high voltage cables," *IEEE Elect. Insul. Mag.*, vol. 13, no. 6, pp. 24–33, Nov. 1997, doi: 10.1109/57.637151.

[7] B. Diban, G. Mazzanti, L. Boyer, and J. Castellon, "Macroscopic conductivity models fit for HVDC cable insulation," JICABLE, Lyon, France, Tech. Rep., Jul. 2023.

[8] G. C. Montanari, G. Mazzanti, F. Palmieri, and B. Bertuzzi, "Mobility evaluation from space charge measurements performed by the pulsed electroacoustic technique," in *Proc. 6th Int. Conf. Properties Appl. Dielectric Mater.*, vol. 1, Jun. 2000, pp. 38–41, doi: 10.1109/ICPADM.2000.875624.

[9] S. L. Roy, G. Teyssèdre, and C. Laurent, "Modelling space charge in a cable geometry," *IEEE Trans. Dielectr. Electr. Insul.*, vol. 23, no. 4, pp. 2361–2367, Aug. 2016, doi: 10.1109/TDEI.2016.7556514.

[10] K. Hallak, F. Baudoin, V. Griseri, F. Bugarin, and S. Segonds, "A new approach for optimizing a bipolar charge transport model for dielectric materials: Theoretical framework," *IEEE Trans. Dielectr. Electr. Insul.*, vol. 28, no. 3, pp. 872–879, Jun. 2021, doi: 10.1109/TDEI.2021.009450.

[11] E. Doedens, E. M. Jarvid, R. Guffond, and Y. V. Serdyuk, "Space charge accumulation at material interfaces in HVDC cable insulation part II—Simulations of charge transport," *Energies*, vol. 13, no. 7, p. 1750, Apr. 2020, doi: 10.3390/en13071750.

[12] B. Diban and G. Mazzanti, "The effect of temperature and stress coefficients of electrical conductivity on the life of HVDC extruded cable insulation subjected to type test conditions," *IEEE Trans. Dielectr. Electr. Insul.*, vol. 27, no. 4, pp. 1313–1321, Aug. 2020.

[13] B. Diban and G. Mazzanti, "The effect of different macroscopic conductivity equations on life estimation of HVDC cables," in *Proc. IEEE Conf. Electr. Insul. Dielectric Phenomena (CEIDP)*, Denver, CO, USA, Oct. 2022, pp. 455–458, doi: 10.1109/CEIDP55452.2022.9985353.

[14] Y. Zhan, G. Chen, and M. Hao, "Space charge modelling in HVDC extruded cable insulation," *IEEE Trans. Dielectr. Electr. Insul.*, vol. 26, no. 1, pp. 43–50, Feb. 2019, doi: 10.1109/TDEI.2018.007413.

[15] Z. Lv, J. Cao, X. Wang, H. Wang, K. Wu, and L. A. Dissado, "Mechanism of space charge formation in cross linked polyethylene (XLPE) under temperature gradient," *IEEE Trans. Dielectr. Electr. Insul.*, vol. 22, no. 6, pp. 3186–3196, Dec. 2015, doi: 10.1109/TDEI.2015.005278.

[16] *CIGRE TB 852–2021 Recommendations for Testing DC Extruded Cable Systems for Power Transmission at a Rated Voltage Up To and Including 800 KV*, 2021.

[17] S. Morita, N. Fuse, T. Takahashi, T. Matsubara, Y. Murata, and N. Hozumi, "Space charge measurement of a 9 mm-thick AC-XLPE cable under steady-state and transient temperature conditions," in *Proc. 9th Int. Conf. Condition Monitor. Diagnosis (CMD)*, Nov. 2022, pp. 122–126.

[18] S. Morita, N. Fuse, T. Takahashi, Y. Murakami, and N. Hozumi, "Examination of electric field distribution measured under 24-hour load cycle condition," in *Proc. Int. Symp. Electr. Insulating Mater. (ISEIM)*, Sep. 2023, pp. 183–186.

[19] W. Xia et al., "Space charge characteristics in 160 kV DC XLPE cable under temperature gradient," *IEEE Trans. Dielectr. Electr. Insul.*, vol. 25, no. 6, pp. 2366–2374, Dec. 2018.

[20] A. T. Hoang, Y. Serdyuk, and S. Gubanski, "Charge transport in LDPE nanocomposites part II—Computational approach," *Polym.*, vol. 8, no. 4, p. 103, 2016.

[21] A. Ndour, S. Le Roy, G. Teyssedre, R. Guffond, and J. Fernandez, "A new model for charges transport and build -up in extruded insulation (XLPE) for HVDC cables," in *Proc. 11 th Int. Conf. Insulated Power Cables*, Jun. 2023, pp. 1–6.

[22] Y. Zhan et al., "Space charge measurement and modelling in cross-linked polyethylene," *Energies*, vol. 13, no. 8, p. 1906, Apr. 2020.

[23] H. Ghorbani, A. Abbasi, M. Jeroense, A. Gustafsson, and M. Saltzer, "Electrical characterization of extruded DC cable insulation—The challenge of scaling," *IEEE Trans. Dielectr. Electr. Insul.*, vol. 24, no. 3, pp. 1465–1475, Jun. 2017.

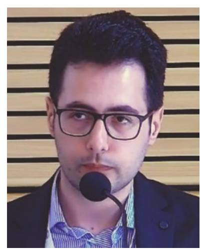

Bassel Diban (Member, IEEE) received the M.Sc. and Ph.D. degrees in electrical energy engineering from the University of Bologna, Bologna, Italy, in 2019 and 2023, respectively.

He is currently a Junior Assistant Professor with the University of Bologna. His research interests are life modeling, reliability, diagnostics of HV insulation, and HVdc cable systems.

Dr. Diban is a member of IEEE DEIS Technical Committee (TC) on "High Voltage Direct-Current (HVdc) cable systems" and CIGRÉ WG B1.91 "Transient Thermal Modeling of Power Cables" (update to IEC 60853).

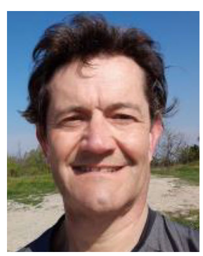

Giovanni Mazzanti (Fellow, IEEE) is a Professor of HV Engineering, Electrical Technologies, and Power Quality at the University of Bologna, Bologna, Italy. He is a Consultant to TERNA (Italian TSO). He has authored more than 350 articles and the book *Extruded Cables for HVdc Transmission: Advances in Research and Development* (Wiley-IEEE, 2013). His research interests are reliability and diagnostics of HV insulation, power quality, renewables, and human exposure to EMF.

Prof. Mazzanti is a member of IEEE PES and DEIS, IEEE DEIS Technical Committee (TC) on "Smart grids," CIGRÉ, CIGRÉ Joint Working Group B4/B1/C4.73 on "Surge and Extended Overvoltage Testing of High Voltage Direct-Current (HVdc) Cable Systems." He is the Chair of the IEEE DEIS TC on "HVdc Cable Systems."